Initiation of deep convection during the early-monsoon sahelian convective boundary layer: an observational study

Cheikh Dione*(1), Marie Lothon(2), Bernard Campistron(2), Fleur Couvreux, Sr(3)
Françoise Guichard(3), Daouda Badiane(1), Saïdou M Sall(1)

(1) Université Cheikh Anta Diop, ESP, LPAO-SF, 5085 Dakar, Sénégal
(2) Université de Toulouse, Laboratoire d'Aérologie - CNRS UMR 5560, Toulouse, France
(3) CNRM-GAME, CNRS, Météo-France, Toulouse, France

1. INTRODUCTION

The triggering factors of deep convection are various and depend on the environmental conditions, like atmospheric vertical structure, as well as surface moisture and temperature heterogeneities [Comer et al., 2007, Taylor and Lebel, 1998, Taylor et al, 2003, Taylor et al., 2011]. Weckwerth et al. [2006] gave a summary of convective storm initiation and evolution based on the results of the International H2O Project (IHOP_2002) experiment [Weckwerth et al., 2004], including frontal zones, gust fronts, boundary-layer rolls, drylines, bores and land surface effect. Wilson et al. [1992] showed that the intersection of convective horizontal rolls and convergence lines can initiate the formation of strong thunderstorms. Conditions for initiation have been analyzed in the Southern Great Plains [Zhang and Klein, 2010] and in the Southwest Amazon region [Lima and Wilson, 2007]. In particular, Lima and Wilson [2007] investigated the possible triddering mechanisms for 315 storms that initiated in the field of view of the radar for a specific day. They found that gust front was dominant mechanism (36%) but that also orography and gust front collision were important mechanisms. The object of this study is to carry on a similar analysis in semi-arid conditions namely over the Sahel with data collected in Niamey, Niger.

The onset period of the monsoon is favorable to study the triggering factors of local deep convection over the Sahelian area. It corresponds to a transition between dry and wet atmosphere and dry and wet surface. At this time of the year, the intertropical discontinuity (ITD) which is the interface between the monsoon flow to the South and the Harmattan flow (hot and dry) to the North it is located a few hundred kilometers North of Niamey. Lothon et al. [2011] showed that on 10 July 2006 convective system initiated around Niamey with a strong role played by surface-atmosphere exchanges and boundary-layer dynamics, confirmed by the numerical study of Couvreux et al. [2012].

In the present study, we extend the observational analysis of the AMMA dataset to the period of 6 to 31 July 2006, in order to further analyse in a more systematic way the main features of the convection observed in Sahelian Africa during the pre-onset and onset of the monsoon, and to further understand the transition from dry convection to shallow convection and from shallow to local deep convection.

A description of the data used in this study is given in section 2. The methods used to characterize the type of convection for July 2006 and the result of the classification are described in section 3. The analysis of triggering factors and processes differentiating the convection days are documented in section 4. Section 5 summarizes and concludes the study.

2. Data

The AMMA campaign which took place in West Africa aimed at improving our knowledge and understanding of the West African monsoon and its variability with an emphasis on daily to interannual time-scales [Redelsperger et al., 2006]. The Special Observing Period centered to the peak of the monsoon took place during summer 2006. Niamey, located in the Sahelian region, lies within one of the three meso-sites of AMMA. For the survey of the Niamey square degree (12.9N - 14.3N; 1.38E - 3.23E), a large set of instruments was deployed [Lebel et al., 2009]. The data used in this study are based on the 3D continuous scans of the Massachusetts Institute of Technology (MIT) radar installed at Niamey and the Atmospheric Radiation Measurement (ARM) mobile facility, with especially: radiosoundings, surface stations, 95 GHz cloud-radar, and Ultra High Frequency (UHF) wind profiler, all deployed nearby the radar and satellite data.

3. Classification of convection day

Based on the data described in the previous section, we have analyzed the occurrence of deep convection in the radius of 50 km around the MIT radar. Four types of convection days were observed over Niamey: (1) dry convection all daytime (FW: Fair weather), (2) shallow convection (SH), (3) afternoon local deep convection (LC)

*corresponding author address: Cheikh DIONE, Centre de Recherches Atmosphériques, 8 route de Lannemezan, 65300 Campistrous, France; *email*: lotm@aero.obs-mip.fr

and (4) propagating deep convection (PC) passing over the area at any time of day.

a Afternoon deep convection

Afternoon deep convection is investigated from the PPI and horizontal cross section of MIT radar reflectivity of 100 km $\times$ 100 km centered on the position of the radar obtained every 10 minutes at different heights. These data allow us to determine the location and time of the onset of convection, and to follow its development and propagation. Deep convection is defined with a minimum threshold on radar reflectivity of 30 dBZ [Wilson and Schreiber, 1986, Wilson and Muller, 1993] and a vertical extension greater than 6 km. To confirm this classification, the IR brightness temperature (233K) from MSG are used in the same area of the MIT radar. The first cell observed in the MIT radar scan volume is tracked every 10 minutes to evaluate how deep the cell develops, how it propagates and whether it generates a circular gust front.

We found nine cases of afternoon locally-initiated deep convection during the 6-31 July period.

b Shallow convection days

Shallow convection days are observed by the MIT radar with a reflectivity smaller than 30 dBZ on the horizontal cross section and a maximum of the 95 GHz cloud-radar reflectivity between 2 and 6 km above ground. In the horizontal cross section the cumulus clouds are found with reflectivity larger than 0 dBZ, which is comfirmed on the MODIS image at 1330 UTC. This type of convection corresponds to the development of cumulus clouds or congestus clouds which do not turn to deeper convection, and dissipate rapidly. Sometime the congestus give small precipitations, for example on 13 July 2006 at Torodi(4 mm between 1400 UTC and 1600 UTC), Southwest of Niamey .

Four cases are found during the studied period.

c Dry convection days

Dry convection is defined when no reflectivity layer maximum is observed in the MIT scanned volume (clear sky in the studied area). This is confirmed with clear sky as seen by the 95 GHz radar. Three dry convection days were found. From one (24 July 2006) of them, the MIT radar was out of work, and 95 GHz cloud-radar and 10.8 μm brightness temperature are used to analyze the occurrence of convection for those days.

d Propagating deep convection

Propagating deep convection is defined when deep convection has been formed outside (usually to the East) of the scan volume of the radar MIT and propagates (westward) across the study area. These convective cells are usually large mesoscale convective systems seen at night or early morning. The sky is usually clear after the passage of such systems. Ten days present this type of situation.

e Results of the classification

Table 1 summarizes the classification of the diurnal convection during our period under study. In summary over the 26 days studied, we found: nine cases of afternoon deep convection (LC), nine cases of propagating deep convection days (PC), four cases of shallow convection days (SH) and tree cases of dry convection days (FW). On 21 July 2006, the atmosphere above the volume scan by the MIT radar is marked by the passage of mid-cloud (seen by the satelite MSG) in early afternoon, and this case has consequently not been classified. Among class (LC) cases, five cases (6, 8, 10, 11 and 12) of local deep convection are observed during the pre-onset and four cases (20, 26, 27 and 28) in the onset period. The transition period between the pre-onset and onset is marked by propagating deep convection or dry convection. For this period, shallow convection is observed either after local or propagating convection days, but never after dry convection days. This classification shows that in addition to large-scale factors (AEWs, squall lines) triggering convection, there are local factors that play an important role in the unfolding of the rainy season in West Africa. The time of initiation of the afternoon deep convection cases (class LC) is determined for each case of this class. Deep convection starts for most of the cases in early afternoon between 1500 and 1700 UTC.

3.1 Convection lines

The role of convection lines in the initiation of deep convection is well documented [Byers and Abraham, 1949, Purdom, 1976, Wilson and Schreiber, 1986, Koch and Ray, 1997, Klüpfel et al., 2012]. Here, convection lines are observed in the horizontal plans of reflectivity deduced from the MIT radar data, as thin lines and cloud lines in the Infrared channel satellite data. For the MIT, we considered reflectivity ranging from 0 to 21 dBZ to identify the position and the length of the convection lines. This threshold on reflectivity also allows us to determine the coherent structure in the convective boundary layer. For satellite data, the brightness temperature is used to confirm the presence of the convection line detected by the radar using a threshold greater than -10^oC.

Figure 1 presents horizontal and vertical cross section of reflectivity at Z= 600 m, and Y= 15 km respectively at 1500, 1550, 1620 and 1640 UTC; and the brightness

Table 1: *Types of convection observed in the volume scan of the C-band radar MIT (100 X 100 km^2) from 6 to 31 July 2006 over Niamey. LC is the afternoon local deep convection day; PC: propagating deep convection all time; SH: shallow convection and FW: dry convection.*

Day of July	06	07	08	09	10	11	12	13	14	15	16	17	18
convection day	LC	PC	LC	PC	LC	LC	LC	SH	PC	PC	FW	PC	FW

Day of July	19	20	21	22	23	24	25	26	27	28	29	30	31
convection day	PC	LC	-	PC	SH	FW	PC	LC/PC	LC	LC	SH	SH	PC

temperature of MSG at 1500, 1545, 1615 and 1645 UTC, on 6 July 2006. Between 1400 and 1500 UTC cumulus clouds developed along the convective line observed to the North of the MIT radar, East-west orientated. Another line is observed in the South of the MIT radar associated with a gust front moving to the North. After 1500 UTC the clouds rapidly developed into the towering cumulus stage on the flank of the Northern line, and few minutes after the radar reflectivity aloft reached 50 dBZ. No deep convection occurred on the Southern line. The length of the line is about 100 km. On this day, and for the two other days that convection line were formed, the CBL was organized in rolls earlier in the morning. The rolls turn to cells in the early afternoon. We found two other days when convection triggers within such a convection line. Therefore, we found that convection lines, growing within the morning clear air roll-organisation, are also found to be precursors of local deep convection in the Sahel.

In the case described above, we found that the deep convection is associated with gust front propagating in all directions, taking a clear circular shape sometime. This gust front is visible on Figure 1b,c. The occurrence of this phenomenon is discussed in the following section.

3.2 Propagating gust fronts

Density current generated by the downdraft of thunderstorms creates a low-level cold pool characterized by large differences between it and the ambient air. The thermodynamic properties of gust fronts and their interactions with the environment air have been studied using tower data [Charba, 1974], Goff [1976], Doppler radar data [Wilson and Schreiber, 1986], Wakimoto [1982], wind profilers with the radio acoustic sounding system (RASS; May [1999]). Benjamin [1968] and Simpson and Britter [1980] defined gust fronts as examples of gravity currents. Wilson and Schreiber [1986] and Lima and Wilson [2007] found that gust fronts were most often associated with convection initiation and could themselves trigger new convective cells.

Gust fronts are observed in the reflectivity radar fields after they move away from the convective cell that generated them and they form a thin line echo in the lower troposphere. Zrnić and Lee [1983] used the 2 dBZ contour to define the gust front echo. Diana and Smith [1987] found that for the nine cases of gust fronts studied, the reflectivity remained smaller than 7 dBZ within the gust front. Horizontal cross sections of reflectivity radar in the low-levels (300 m to 600 m) are used here to observe the formation and propagation of the gust fronts in the volume scanned by the MIT radar, combined with pressure rise, wind shift, wind surge, and temperature drop deduced from the meteorological station around Niamey, when appropriate. Vertical cross section of reflectivity approximately delimited the height of the density current.

Figure 2 shows the reflectivity interpolated in horizontal cross sections at 300 m height and vertical zonal cross sections 15 km to the South of the MIT radar, at 1610, 1640 and 1730 UTC on 11 July 2006. The first deep convection cell developed at 1510 UTC, 20 km to the South of the MIT radar (X= 0 km , Y= -20 km not shown). It propagated Southwestward, became very deep and generated a circular gust front at 1610 UTC (Fig. 2a). New cells are observed a few minutes in the volume swept by the density current up to 1500 m by place. They propagated in the same direction than the first cell but dissipated shortly later (Fig. 2b,c). This case was very similar to the case of the day before, studied by Lothon et al. [2011] in which the gust front initiated several other convective cells that had life span less than 2 hours. With 10 and 11 July, we found five other days among the nine cases of class LC, when gust fronts generated new cells. Another day had a gust front that did not generate new cells.

For two locally-initiated deep convection associated with gust front, we were able to determine the potential of the gust front to trigger news cells. The case of 10 and 11 July are investigated here to verify a simple model proposed by Grandpeix and Lafore [2010] to evaluate the characteristcs of the density current. In Grandpeix and Lafore [2010] parameterization, density currents are defined by their density within the grid cell, their fractional area σ_w, their depth h_w, the change of temperature and water vapor mixing ratio within the wake relative to their environment, their expansion rate C_*, and their propagation speed V_w. C_* is thus the mean spreading speed of the wake leading edge (gust front here), while V_w is the

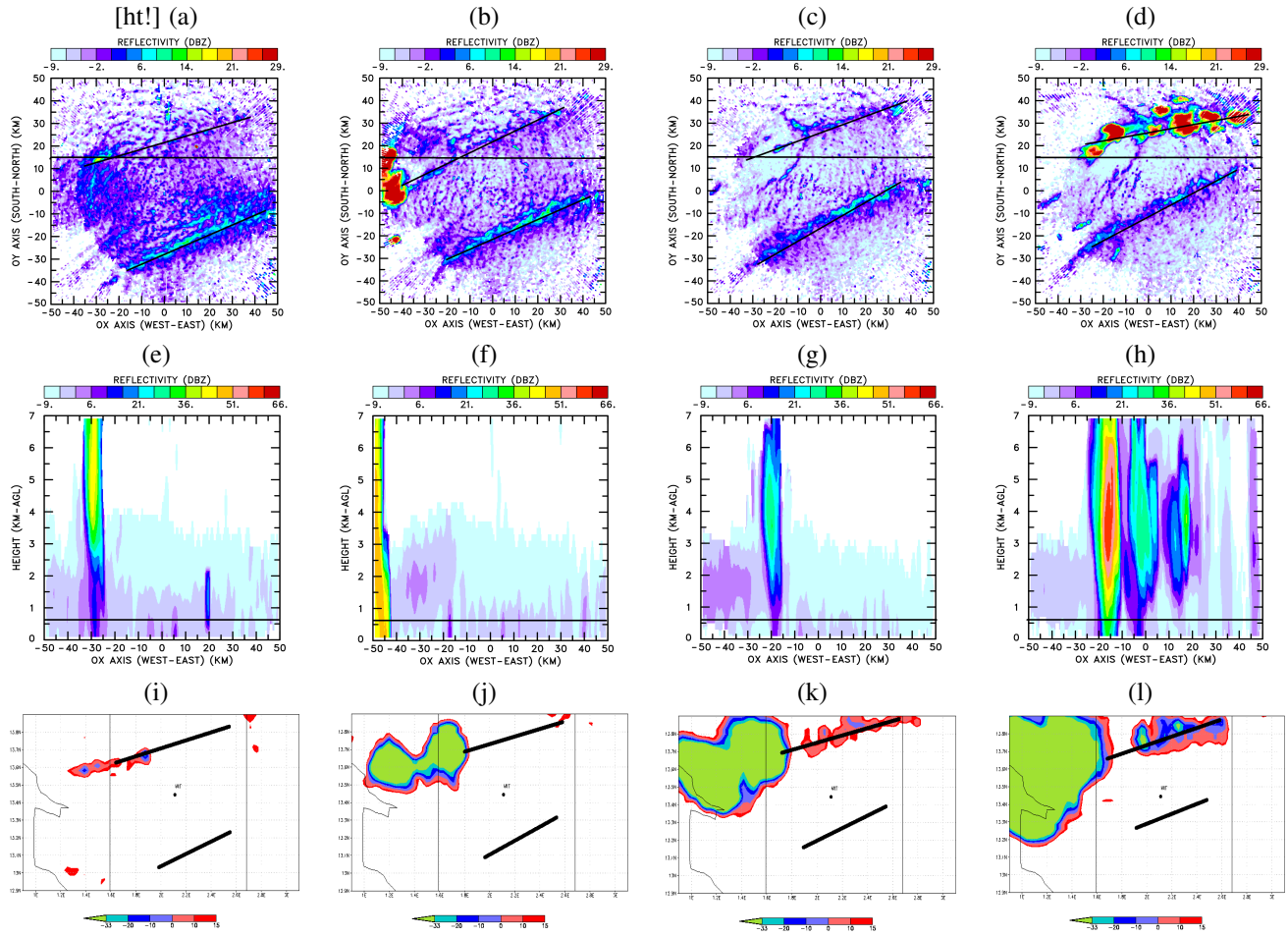

Figure 1: *Reflectivity interpolated in (first row) horizontal cross section at Z=600 m AGL, (second row) vertical cross section at Y=15 km, at (a, e) 1500; (b, f) 1550; (c, g) 1620 and (d, h) 1640 UTC and (last row) Brightness temperature from MSG satellite at (i) 1500; (j) 1545; (k) 1615 and (l) 1645 UTC on 06 July 2006. The MIT radar is positioned at the reference point (X=0, Y=0). Here R_{xy}=600 m and R_z=350 m are used for the horizontal section and R_{xy}=1000 m and R_z=1000 m for the vertical section. The northern black line indicates orientation of the convection line observed. The square on satellite images indicates the scan volume (100 × 100 km^2) of the MIT radar. The southern black line indicates a gust front created by another cell to the South.*

translation speed of the whole cold pool.

The wake potential energy (WAPE) is defined as the mean potential energy deficit in the wake region:

$$WAPE = -g \int_0^{h_w} \frac{\delta\theta_v(z)}{\overline{\theta}_v} dz \qquad (1)$$

where θ_v is the virtual potential temperature and h_w is the mean wake depth. $\overline{\theta}_v$ is the mean virtual potential temperature, and $\delta\theta$ is the difference between the virtual potential temperature in the cold pool and the virtual potential temperature of the environment:

$$\delta\theta_v(z) = \theta_{v_w} - \overline{\theta}_v \qquad (2)$$

Here $\overline{\theta}_v$ is assumed constant in the boundary layer due to mixing, and h_w is the mean wake depth, defined by $\delta\theta_v(z = h_w) = 0$.

Following Von Kármán [1940], the wake spreading speed is proportional to the square root of the WAPE:

$$C_* = k_* \sqrt{2WAPE} \qquad (3)$$

Where k_* is a coefficient. Goff [1976] gave a simple equation to estimate C_* as a function of the maximum speed observed normal to the front:

$$C_* = 0.67 * U \qquad (4)$$

In our cases, we evaluate the expansion rate of a single almost circular density current, from the change of area covered by the wake with time. On the horizontal cross

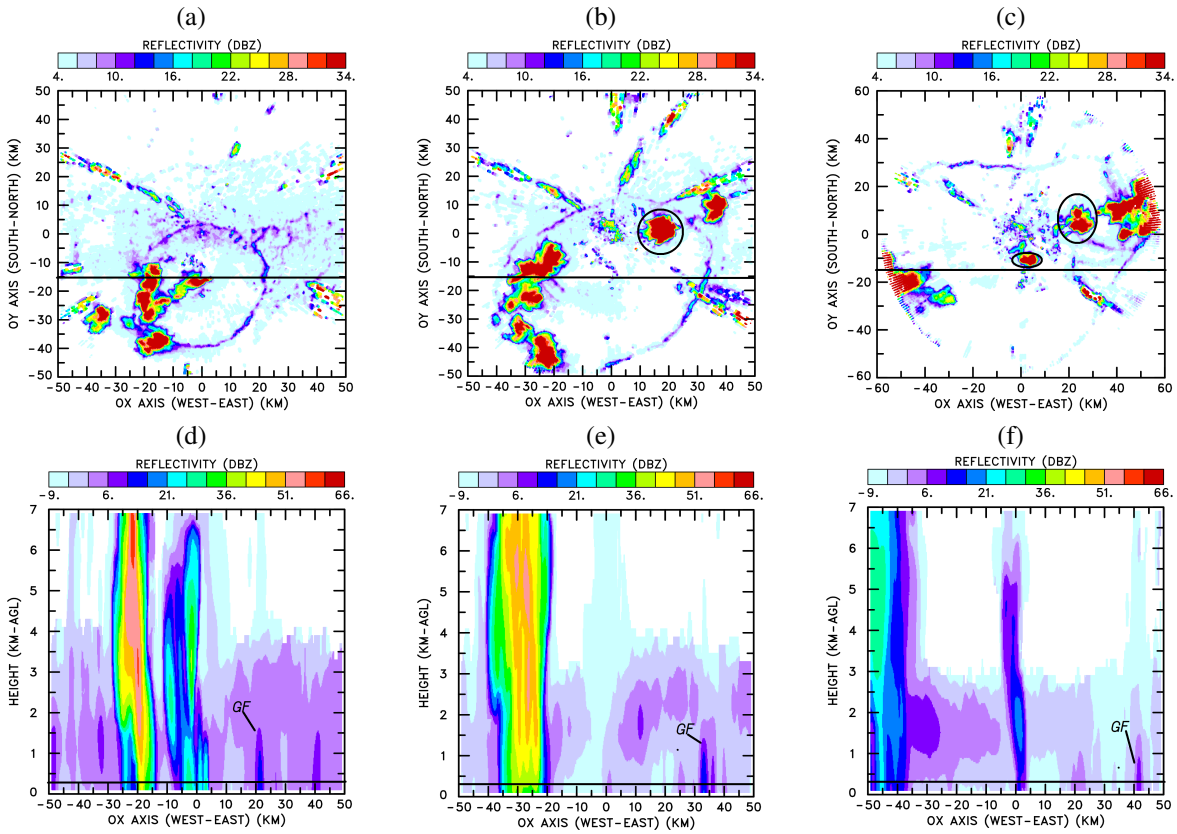

Figure 2: *(top) Horizontal and (bottom) vertical cross section of Reflectivity interpolated in (first row) at Z= 300 m AGL and (second row) at Y=-15 km, at (a, d) 1610, (b, e) 1640 and (c, f) 1730 UTC on 11 July 2006. The MIT radar is positioned at the reference point (X= 0, Y= 0). The radii of influence used here for the interpolation are R_{xy}= 600 m and R_z= 350 m for horizontal cross section and R_{xy}= 1000 m and R_z= 1000 m for the vertical cross section. Cells triggered by the gust front are circled in black. "GF" indicates the top of the Gust front. In (a), (b), and (c) a minimum of reflectivity radar of 4 dBZ on the colorscale is used to mask the clear air organisation and to point out the clear signature of the gust front.*

section of reflectivity radar (see Fig. 2) the area swept by the density current are slightly deformed as elliptic form. However, in order to test this model, we assume the wake area to be circular. We processed the images in a way similar to that shown in this figure, coloring the pixels that are within the circular gust front black and the pixels that are off the wake white. This enabled us to estimate the area covered by the wake and the cell, relative to the 100 km $\times$ 100 km window considered around the radar (see [Lothon et al., 2011]), and deduced the extension coefficient for the two cases.

Figure 3.2 shows the vertical profiles of virtual potential temperature deduced from the radiosounding at 1730 UTC. These profiles are used to estimate the depth of the density current and to evaluate the WAPE. Our results on this method are shown in Table 3.2. For the two days, we found k_* equal to 0.39 and 0.44 respectively for 10 and 11 July. These results are consistent with Grandpeix and Lafore [2010] who found values of this coefficient between 0.33 and 0.7 for a possible triggering of new deep convective cells by the density currents.

Table 2: *Characteristics of the Density current for 10 and 11 July 2006.*

Day	h_w (m)	$\bar{\theta}_v$ (K)	WAPE (J Kg^{-1})	C_* (m s^{-1})	k_*
10 July	1500	313	36.3	3.35	0.39
11 July	1620	313.6	38.5	4	0.45

4. Analysis of the triggering factors of deep convection

In this section, we analyse the triggering factors that may differentiate convection classes observed over Ni-

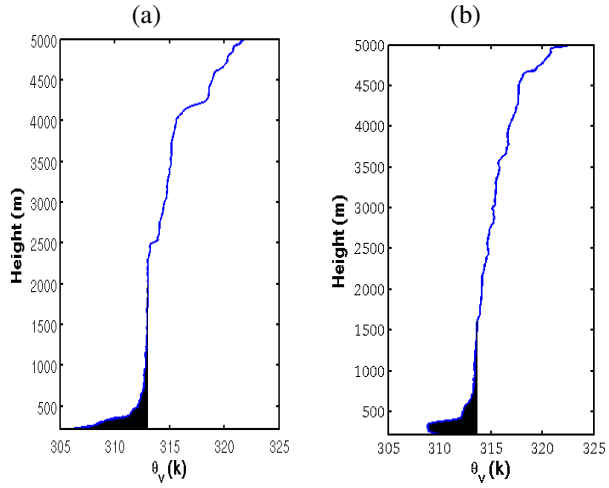

Figure 3: *Vertical profiles of virtual potential temperature at 1730 UTC on (a) 10 July and (b) 11 July. The WAPE is represented on the two profiles by the black shaded area.*

amey.

4.1 Atmospheric stability parameters

The convective available potential energy (CAPE) and convective inhibition (CIN) were calculated using the lowest 100 mb average virtual potential temperature-based parcel calculations [Doswell and Rasmussen, 1994]. Figure 4 represents the CIN as a function of the CAPE at 0530 and 1130 UTC for all cases of convection days.

At 0530 UTC, it is very difficult to predict the afternoon local deep convection. Many cases of any class have $CAPE > 500\ J\ kg^{-1}$, but $|CIN| < 200\ J\ kg^{-1}$ which is unfavorable for deep convection. Also several cases have $CAPE < 500\ J\ kg^{-1}$ and $|CIN| > 180\ J\ kg^{-1}$ unfavorable for deep convection (see Fig. 4 at 0530 UTC). The high values of CAPE for class PC are due to the instability of the atmosphere before the passage of the MCSs. The deep convection usually initiates in the late afternoon East of Niamey and propagates westward, passing through the volume scan of the MIT radar at night or early morning.

At 1130 UTC, classes PC and FW have $CAPE < 500\ J\ kg^{-1}$ and $|CIN| > 200\ J\ kg^{-1}$ unfavorable to deep convection. The conditions start to become favorable for most cases of class LC and SH with $CAPE > 600\ J\ kg^{-1}$ and $|CIN| < 180\ J\ kg^{-1}$. There is a very high value of CAPE over 6000 $J\ kg^{-1}$ for only one case of afternoon local deep convection (28 July 2006). Thus at this time of day, we may separate (LC,SH) from (PC,FW), but it is still difficult to distinguish shallow convection days from afternoon local deep convection days (see Fig. 4).

Between 0530 and 1130 UTC the CAPE of PC cases decreases significantly. For the cases of FW the decrease in CIN is more significant than the change in CAPE. Classes LC and SH have a significant decrease of CIN and often a decrease of CAPE (Fig. 4).

By use of the convective triggering potential and a humidity index HI_{low} defined by Findell and Eltahir [2003a], we tried to classify the types of convection using this theory, noticing that the surface is generally dry during the study period. We conclude that it is very difficult to predict at 0530 UTC the type of convection that will be formed during the day, based on the CTP and HI_{low} indexes (not shown).

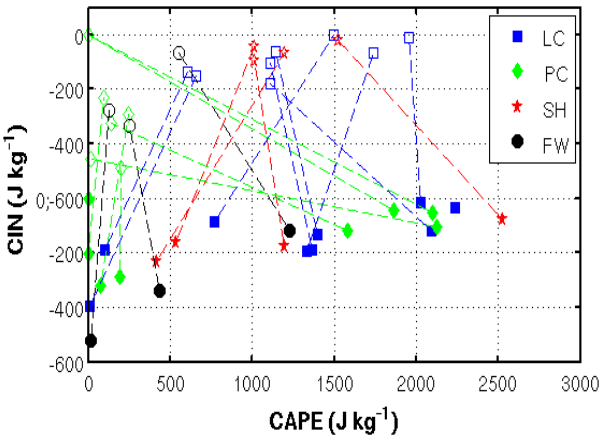

Figure 4: *CIN as a function of CAPE at 0530 (filled symbols) and 1130 UTC (empty symbols) for all days from 6 to 31 July 2006: blue squares represent cases of local deep convection, green diamonds cases of propagating deep convection, red stars cases of shallow convection and black circle cases of dry convection.*

4.2 Growth of the convective boundary-layer

Based on Hapex-Sahel dataset, Wai et al. [1997] found that the boundary layer responds quickly to the transition from wet to dry seasons and the same was observed by Gounou et al. [2012] for the onset period. Kohler et al. [2010] found that the diurnal development of convective instability was dominated by the CBL evolution and controlled by the transfers in the mid or upper troposphere.

The diurnal cycle of the surface heat fluxes drives the growth of the atmospheric boundary layer. In this part, we analyse the processes in the low-level from surface to 4 km above.

Figure 5 shows the vertical profiles in the low-levels for potential temperature θ and water vapor mixing ratio at 0530 and 1130 UTC for classes SH and FW.

At 0530 UTC the vertical profiles of θ are relatively similar in the two classes of convection. It is characterized by a cool stable layer in the low-levels. However, the inversion layer is in general larger for the cases of dry convection than those of shallow, a wet nocturnal surface layer with mixing ratio greater than 15 g kg^{-1} is observed for all cases of the two classes. Cases of class FW often have a smaller mixing ratio than those of class SH in the lower troposphere.

Through the heating of the surface due to solar radiation, there is a significant transformation of air mass between 0530 and 1130 UTC (see Fig. 5c,d). At 1130 UTC the mixed layer differs from one class of convection to the other. Cases of FW have cooler and thinner CBL than those of classes SH and LC (not shown). The mixed layer of SH cases have all deeper CBL, with Zi greater than 1200 m (see Fig. 5c). The low troposphere is drier for the FW cases at that time, as observed at 0530 UTC. This dry air noted in the low-levels for FW is unfavorable for the formation of cumulus cloud at the top of the boundary layer, because the level of condensation of the air mass is then higher than the CBL top reached.

Note that the moisture supplied by the nocturnal jet is distributed in the boundary layer by the diurnal convection for class SH and LC, and in a lesser extent for class FW. Between 0530 and 1130 UTC, cases of LC (not shown) present wet and deep mixed layer (not shown).

Figure 6 shows the composite diurnal cycle of the atmospheric boundary layer (ABL) depth for all convection classes, based on the estimates of Z_i by UHF wind profiler. On propagating deep convection days, the ABL height grows slowly before reaching about 1 km in the afternoon. On dry convection days, the ABL height grows moderately and reaches around 1.5 km after 1530 UTC, and continues to rise. On shallow convection and afternoon local deep convection days, the ABL height grows more rapidly. However, the ABL height continues to grow between 1300 and 1800 UTC for class LC, while Z_i tends to level off for cases of class SH.

The growth of the convective atmospheric boundary layer seems to be a key variable for distinguishing afternoon local deep convection days from shallow convection days.

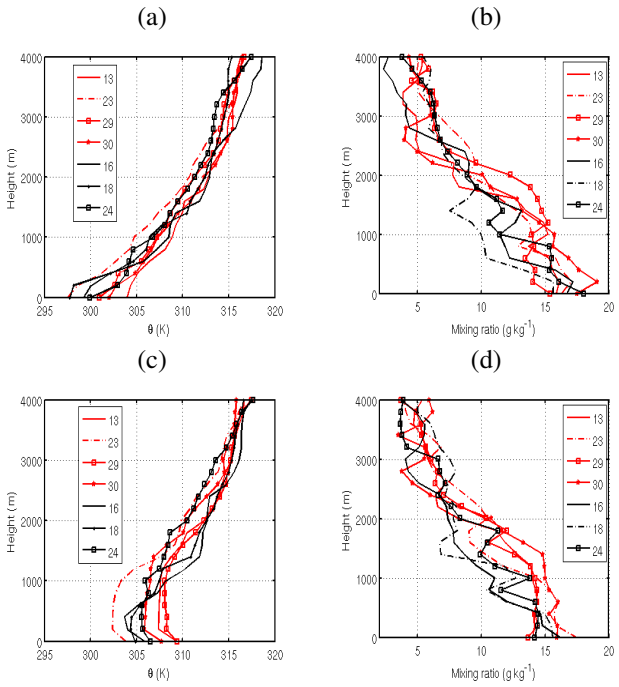

Figure 5: *Vertical profiles of (left panels) potential temperature θ and (right panels) mixing ratio at (first row) 0530 UTC and (second row) 1130 UTC: (red line) shallow convection days, (black line) dry convection days.*

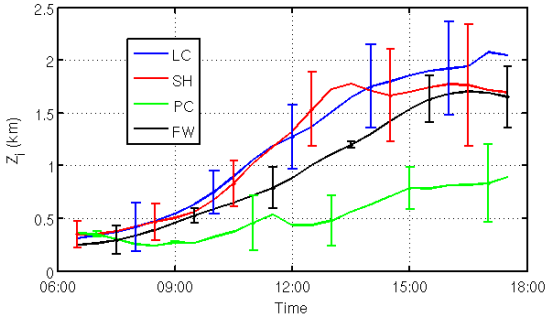

Figure 6: *Composite diurnal cycle of the atmospheric boundary layer (ABL) height for each class deduced from the UHF wind profiler: (blue line) afternoon local deep convection days, (red line) shallow convection days, (green line) propagating deep convection days and (black line) dry convection all days. We considered that the boundary-layer depth is not defined during a rainfall event.*

5. Summary and Conclusions

The MIT radar data for AMMA campaign 2006 completed with satellite data, 95 GHz cloud radar, radiosoundings, UHF wind profiler has been used to characterize the diurnal cycle into different atmospheric convection regimes in the Sahel over Niamey. This study is based on the analysis of horizontal and vertical cross section of reflectivity of the MIT radar in the scanned volume (100 × 100 km^2 centered on the position of the radar) and confirmed by the satellite data in the same area for 26 days of July 2006. Four types of convection regimes have been identified: (FW) dry convection all daytime (3 cases), (SH) shallow convection (4), (LC) afternoon locally-initiated deep convection(9) and (PC) propagating deep convection (10). We found a large occurrence

of local deep convection during this period, as large as that of propagating MCS passing through the area. Our results also confirmed the validity of the model proposed by Grandpeix and Lafore [2010].

The capability of the MIT radar to observe the gust fronts and convection lines is demonstrated. The data suggest the important role of the convection lines as precursors of afternoon locally-initiated deep convection in the Sahel. We find 3 occurrences of the convection line over Niamey during the study period, over the 9 cases observed. Most of the cases of local deep convection are associated with gust fronts that trigger new cells in the area swept by the density current. For two days (10 and 11 July), we calculated the wape available potential energy and demonstrated the capability of the wakes to trigger news convective cells.

The analysis of the atmospheric instability factors the CAPE, CIN, CTP and HI_{low} shows the difficulties to predict the deep convection occurrence with those parameters alone. Even at 1130 UTC CAPE and CIN help to predict the convection but do not separate classes of local deep convection from shallow convection. CTP and HI_{low} did not show clearly-defined regimes, as those put into evidence by Findell and Eltahir [2003a].

Classes FW, SH and LC show several similar conditions that are favorable for deep convection, but FW has smaller convective boundary layer (CBL) growth, relatively to the 2 other classes. The CBL is also cooler and dryer than for SH and LC cases. LC cases have the deepest, warmest and wettest CBL. SH and LC cases are distinguished only with the existence of a significant divergence (not shown) above the CBL for class SH, while convergence is observed for LC. FW also shows divergence above the CBL, but smaller than for class SH.

We have observed that for many of the LC cases considered here and in agreement with Taylor et al. [2011], the deep convective cells have initiated on a warm surface area relatively to their mesoscale surrounding (not shown). Future works will consider the same set of cases to further analysis the role of the surface heterogeneity to trigger deep convection on favored spots.

Acknowledgements

Laboratoire d'Aérologie is funded by INSU-CNRS and the University of Toulouse. Based on a French initiative, AMMA was built by an international scientific group and is currently funded by a large number of agencies, especially from France, the United Kingdom, the United States, and Africa. It has been the beneficiary of a major financial contribution from the European Communitys Sixth Framework Research Program. (Detailed information on scientific coordination and funding is available on the AMMA International Web site at http://www.amma-international.org.) The authors also thank the Massachusetts Institute of Technology and NASA Hydrology for supporting the operation of the radar in Niamey. We thank Brian Russell for his organization and archival of the MIT radar data. We thank the Atmospheric Radiation Measurement Facility for operating the UHF wind profiler, radiosoundings and surface stations, and for supplying the data. The main author of this article thanks the SCAC (Service de Coopration et d'Action Culturelle) of the French embassy in Dakar to have accorded a scholarship and the PCSI (Programme de Coopération Scientifique Interuniversitaire) programm supported by AUF (Agence Universitaire de la Francophonie) who has funded a tree-month internship in France.

REFERENCES

Benjamin, TB., 1968: Gravity currents and related phenomena. J. Fluid. Mech., 31(2), 209-248.

Byers, H. R., and R. R. Braham, 1949: The Thunderstorm. U.S. Govt. Printing Office, 287 pp.

Charba, J., 1974: Application of gravity current model to analysis of squall line gust front. Mon. Wea. Rev., 102, 140-156.

Comer, R. E., A. Slingo, and R. P. Allan, 2007: Observations of the diurnal cycle of outgoing longwave radiation from the Geostationary Earth Radiation Budget instrument. Geophys. Res. Lett., 34, L02823, doi:10.1029/2006GL028229.

Couvreux, F., C. Rio, F. Guichard, M. Lothon, G. Canut, D. Bouniol, A. Gounou, 2012: Initiation of daytime local convection in a semi-arid region analysed with high-resolution simulations and AMMA observations. Quart. J. Roy. Meteor. Soc., 138, 56-71.

Diana, L. K., and D. R. Smith, 1987: Gust fronts as detected by Doppler radar. Mon. Wea. Rev., 115, 905-917.

Doswell, C. A. III., and E. N. Rasmussen, 1994: The effect of neglecting the virtual temperature correction on CAPE calculations. Wea. Forecasting, 2, 625-629.

Findell, K. L., and A. B. Eltahir, 2003: Atmospheric Controls on Soil MoistureBoundary Layer Interactions. Part I: Framework Development. J. Hydrometeo. 4, 552-569.

Goff, CR., 1976: Vertical Structure of Thunderstorm Outflows. Mon. Wea. Rev., 104, 1429-1440.

Gounou, A., F. Guichard, F. Couvreux, 2012: Observations of Diurnal Cycles Over aWest African Meridional Transect: Pre-Monsoon and Full-Monsoon Seasons. Bound. Layer Meteorol., DOI 10.1007/s10546-012-9723-8.

Grandpeix, J. Y. and J. P. Lafore, 2010: A density current parameterization coupled with Emanuels convection scheme. Part I: The models. J. Atmos. Sci., 67, 881-897.

Koch, S. E., and C. A. Ray, 1997: Mesoanalysis of summertime convergence zones in central and eastern North Carolina. Wea. Forecasting, 12, 56-77.

Kohler, M., N. Kalthoff, and C. Kottmeier, 2010: The impact of soil moisture modifications on CBL characteristics in the West Africa: A case-study from the AMMA campaign. Quart. J. Roy. Meteor. Soc., 136, 442-455.

Klüpfel, V., N. Kalthoff, L. Gantner, and C. M. Taylor, 2012: Convergence zones and their impact on the initiation of a mesoscale convective system in West Africa. Q. J. R. Meteorol. Soc.. doi: 10.1002/qj.979

Lebel, T., D. J. Parker, C. Flamant, B. Bourles, B. Marticorena, E. Mougin, C. Peugeot, A. Diedhiou, J. M. Haywood, J. B. Ngamini, J. Polcher, J. L. Redelsperger, C. D. Thorncroft, 2009: The AMMA field campaigns: Multiscale and multidisciplinary observations in the West African region. Quart. J. Roy. Meteor. Soc. This issue: in revision.

Lima, M. A., and W. Wilson, 2007: Convection Storm Initiation in a Moist Tropical Environment. Mon. Wea. Rev., 136, 1847-1864.

Lothon, M., B. Campistron, M. Chong, F. Couvreux, F. Guichard, C. Rio, E. Williams, 2011: Life Cycle of a Mesoscale Circular Gust Front Observed by a C-Band Doppler Radar in West Africa. Mon. Wea. Rev., 139, 1370-1388.

May, PT., 1999: Thermodynamic and Vertical Velocity Structure of Two Gust Fronts Observed with a Wind Profiler/RASS during MCTEX. Mon. Wea. Rev., 127, 1796-1807.

Purdom, J. F. W., 1976: Some uses of high resolution GOES imagery in the mesoscale forecasting of convection and its behavior. Mon. Wea Rev., 104, 1474-1483.

Redelsperger, J. L., D. Thorncroft, A. Diedhiou, T. Lebel, D. Parker, J. Polcher, 2006: African monsoon multiplidisciplinary analysis: An international research project and field campaign. Bull. Am. Meteorol. Soc. 87, 1739-1746.

Simpson, J. E., and R. E. Britter, 1980: A laboratory model of an atmospheric mesofront. Q. J. R. Met. Soc. 106, 485-500.

Taylor CM, Gounou A, Guichard F, Harris PP, Ellis RJ, Couvreux F, Kauwe MD. 2011. *Frequency of Sahelian storm initiation enhanced over mesoscale soil-moisture patterns*. Nature Geoscience., 4, 430-433 (2011) doi:10.1038/ngeo1173.

Taylor, C. M., D. J. Parker, R. R. Burton, and C. D. Thorncroft, 2003: Linking boundary-layer variability with convection: A case-study from JET2000. Quart. J. Roy. Meteor. Soc., 129, 2233-2253.

Taylor, C. M., T. Lebel, 1998: Observational evidence of persistent convective-scale rainfall patterns. Mon. Weather Rev. 126: 1597-1607.

Von Kármán, T., 1940: The engineer grapples with nonlinear problems. Bull. Amer. Math. Soc., 46, 615-683.

Wai, M. M. K., E. A. Smith, P. Beemoulin, A. D. Culf, A. J. Dolman, and T. Lebel, 1997: Variability in boundary layer structure during HAPEX-Sahel wet-dry season transition. J. Hydrology, 188-189, 965-997.

Wakimoto, R. M., 1982: The life cycle of thunderstorm gust fronts as viewed with Doppler radar and rawinsonde data. Mon. Wea. Rev., 110, 1060-1082.

Weckwerth, T., and Coauthors, 2004: An overview of the International H20 Project (IHOP_2002) and some preliminary highlights. Bull. Amer. Meteor. Soc., 85, 253-277.

Weckwerth, T., and D. B. Parsons, 2006: A review of convection initiation and motivation for IHOP_2002. Mon. Wea. Rev., 134, 5-22.

Wilson, J. W., G. B. Foote, N. A. Crook, J. C. Fankhauser, C. G. Wade, J. D. Tuttle, C. K. and Mueller, 1992: The role of boundary layer convergence zones and horizontal rolls in the initiation of thunderstorms: A case study. Mon. Wea. Rev., 120, 1785-1815.

Wilson, J. W., and C. K Mueller, 1993: Nowcasts of thunderstorm initiation evolution. Wea. Forecasting., 8, 113-131.

Wilson, J. W., and W. E. Schreiber, 1986: Initiation of convective storms at radar-observed boundary-layer convergences lines. Mon. Wea. Rev., 114, 2516-2536.

Zhang, Y., S. A. Klein, 2010: Mechanisms Affecting the Transition from Shallow to Deep Convection over Land: Inferences from Observations of the Diurnal Cycle Collected at the ARM Southern Great Plains Site. J. Atmos. Sci., 67, 2943-2959.

Zrnić, D. S., and J. L. Lee, 1983: Investigation of the detectability and lifetime of gust fronts and other weather

hazards to aviation. FAA Rep. No. DOT/FAA/PM-83/33, 58pp.[Available through NTIS, Springfield, VA 22151, NTIS No. AD-A141 552.]